Preparation of magnetic porous ceramsite and its application in biological aerated filters

Teng Bao[a,b], Tianhu Chen[a*], Haibo Liu[a, b],Dong Chen[a, b], Chengsong Qing[a], Ray L. Frost[b*]

[a] Laboratory for Nanominerals and Environmental Material, School of Resource and Environmental Engineering, Hefei University of Technology, China.

[b]School of Chemistry, Physics and Mechanical Engineering, Science and Engineering Faculty, Queensland University of Technology, Australia.

[*]Author to whom correspondence should be addressed: TianhuChen,chentianh@hfut.edu.cn.; Ray L. Frost, r.frost@qut.edu.au

Abstract:

Ceramsite plays a significant role as a biological aerated filter (BAF) in the treatment of wastewater. In this study, a mixture of goethite, sawdust and palygorskite clay was thermally treated to form magnetic porous ceramsite (MPC). An optimization experiment was conducted to measure the compressive strength of the MPC. X-ray diffraction (XRD), scanning electron microscopy (SEM), and polarizing microscopy (PM) characterized the pore structure of the MPC. The results show that a combination of goethite, sawdust and palygorskite clay with a mass ratio of 10:2:5 is suitable for the formation of MPC. The compressive strength of MPC conforms to the Chinese national industrial standard (CJ/T 299-2008) for wastewater treatment. The SEM and PM results also show that the uniform and interconnected pores in MPC were well suited for microbial growth. The MPC produced in this study can serve as a biomedium for advanced wastewater treatment.

Keywords: Magnetic porous ceramsite (MPC); Goethite; Palygorskite clay; Biological aerated filter (BAF); Biofilm;

1. Introduction

Porous ceramsite is an effective media used in biological aerated filters (BAFs) for the treatment of wastewater [1]. The characteristics of porous ceramsite are related to the initial capital outlay, process design, and operation mode of BAFs. These characteristics also improve the efficiency and daily running costs such as backwashing and air influx. Mineral supports for porous ceramsite include zeolite, clay, sand, macadam, coke, anthracite coal, and plastic materials, such as polyethylene and polystyrene [2, 3]. Studies in China during the late 1980s indicated that BAFs which contained expanded clay as a biofilm support could achieve superior substrate removal compared to sand and plastic media of similar dimensions [4].

Sawdust is a byproduct of timber processing and extraction. In China, the annual production of sawdust amounts to nearly 180 million tons and is increasing by 6 to 8% per year [5]. The generation of sawdust in earlier years has resulted in huge accumulations in many parts of China. The management of sawdust waste is a heavy economic burden to industry [6], and it is important to utilize or add value to waste sawdust. Lu et al. [7] reported that at high sintering temperatures the lignin and cellulose in sawdust can be converted into a carbonaceous porous material which could be used as a cellular material. However, to the best of our knowledge, only a small number of studies have reported the use of sawdust as a porous material [8].

Palygorskite is a natural magnesium-aluminum silicate clay mineral with a diameter of 30-50 nm. It is known to contain continuous two-dimensional tetrahedral sheets, but differs from other layered silicates due to its lack of continuous octahedral sheets. The tetrahedral basal oxygen atoms invert apical directions at regular intervals and thereby forming talc-like ribbons. It has a high surface area, viscosity, and porosity as well as significant thermal resistance and chemical inertness. In China, palygorskite resources are abundant in the eastern part of Anhui Province and western part of Jiangsu Province. It is an excellent absorbent, and recent attention has focused on the utilization of palygorskite [9-11].

To the best of our knowledge, there is no study investigating palygorskite for the production of ceramsite. The compositional and structural variations of ceramsite

obtained in previous studies were attributed to many factors such as sintering temperature, sintering time, and the ratio of palygorskite/goethite. However, no studies have yet been conducted to investigate the impact of the specific and important constituents on the characteristics of ceramsite. As one of these components, palygorskite may strongly affect the bloating behavior and crystal formation of ceramsite during the heat treatment process.

The application of magnetic materials to solve environmental problems has received considerable attention in recent years due to their ability to separate substances in a liquid medium after adsorption [12-16]. Although magnetite (Fe_3O_4) has been used to precipitate heterogeneous calcium phosphate, its use in the context of environmental pollution has not received much attention. Scarce information is available on the potential application of magnetite as a phosphate sorbent [17].Magnetized BAF has been used in treating wastewater, mostly to separate solids or attached microorganisms from effluent. Reports indicate that there was an increase in bacterial activity during the separation process[18].

The selection of a suitable BAF medium is critical in process design and operation if the required effluent standards are to be met. The characteristics of the filter media can significantly affect the initial investment and operational costs. The selection of the BAF media will depend on many factors, including its resistance to microbial degradation, its mechanical strength, the type of fluid used, its surface characteristics, and its cost. In this study, the MPC was prepared by sintering a mixture of goethite, sawdust, and palygorskite. Sawdust was treated at 400-800 $^{\circ}C$ to produce a desirable porous material. During sintering, goethite is transformed into magnetite in the presence of H_2 gas emitted during pyrolysis at 400 $^{\circ}C$ [19]. The formation of an interior porosity improves microbial growth. This study may lead to a promising new method for the preparation of biofilter carriers.

To validate this hypothesis, the present study has been conducted to: (i) utilize palygorskite/goethite and sawdust for the production of ceramsite; (ii) investigate the effect of palygorskite and sawdust on the physical characteristics (porosity) of ceramsite; (iii) characterize the ceramsite within the optimal content ranges of

palygorskite/goethite and sawdust via thermal analysis, morphological structure analysis, X-ray diffraction, and compressive strength; (iv) analyze the sintering mechanisms; and (v) establish effective evaluation parameters.

2. Methods and Materials

2.1. Material

The raw palygorskite came from Crown Hill located in the city of Mingguang , Anhui province, China. Sawdust was sampled from the city of Hefei, Anhui province, China. Goethite was obtained from the city of Zhenjiang, Jiangsu province, China. The particle size after extrusion, cutting, and crushing was less than 0.074 mm. Commercial ceramsite (CC) was obtained from the city of Ma'anshan, Anhui Province, China. The characteristics of MPC and CC are specified in Table 5. MPC were superior to CC in many ways, including porosity, specific surface area, and apparent density (Table 5).

2.2. Preparation of magnetic porous ceramsite (MPC)

The preparation of MPC includes the following steps:

1). The mixture of goethite, sawdust, and palygorskite with the experimental mass ratio was placed in a small coating machine which produced round granules with a diameter of 7-13 mm.

2). The products were dried at 110 $^{\circ}$C.

3). The composite iron oxide particles were put in a 2 L quartz tube reactor and heated at 500, 600, 700, and 800 $^{\circ}$C. Each of these temperatures was maintained for 0.5-4 h under a N_2 atmosphere at a flow rate of 30 mL/min.

4). The annealed MPC was cooled to room temperature over 12 h.

5). The synthesized MPC was stored in a vacuum desiccator for future analysis.

2.3. The application of MPC in biological aerated filters (BAF)

Backwashing is a very important step in BAF operation. BAFs need to be optimized to reduce the water consumption and energy cost of backwashing. To

achieve this, the current methods attempt to reduce the apparent density of biofilter carriers. The increase in apparent density facilitates the merger of well-developed microbial membranes with biofilter carriers in the BAF. This increases the inefficiency of BAF backwashing and may result in significant BAF short-circuited current. In addition, it will create to excessive BAF backwashing. These effects can lead to excessive biofilm detachment which can result in deterioration of effluent water quality.

In this research, magnetic porous ceramsite (MPC) is attracted to the electromagnetic iron-separator (Fig. 1). The experiments showed that the electromagnetic iron-separator can shift the MPC in the BAF. The MPC is moved to a certain height and then the electricity supply is switched off and the MPC sheds biofilm. At the same time, the MPC collide into each other and accumulate to form voids that facilitates regeneration ability. This method of making MPC voids obviates the need for backwashing, and the restoration process is much faster than combined action gas-water backwashing.

2.4. Characterization

The multi-point Brunauer–Emmett–Teller (BET) surface area of MPC was measured using a Quantachrome Nova 3000e automated surface area analyzer. X-ray fluorescence (XRF) chemical composition was measured on a Shimadzu XRF-1800 with Rh radiation. X-ray diffraction (XRD) was performed using a Rigaku powder diffractometer with Cu Kα radiation. The tube voltage was 40 kV and the current was 100 mA. The XRD diffraction patterns were taken in the range of 5-70 °C at a scan speed of 4° min^{-1}. Phase identification (Search-Match) was carried out by comparison with those included in the Joint Committee of Powder Diffraction Standards (JCPDS) database. Elemental analyses of the sample were carried out by a VARIO ELIII analyzer (Elemental analysis system Co. Ltd., Germany). Magnetic susceptibility analyses of the samples were carried out via a Bartinton MS2 analyzer.

The thermal behavior of samples was examined by DTA-TGA7300 using an EXSTAR simultaneous DTA-TGA7300 analyzer while the samples were heated at a

rate of 8 ^{o}C/min from 20 to 700 ^{o}C with nitrogen atmosphere at 100 mL/min. Samples ranged from 4 to 10 mg in mass, and they were compacted into a Pt-Rh crucible with 20 taps.

In the biological structures analysis, selected MPC were sputter coated with gold and its surface morphology was examined using a Scanning Electron Microscope (SEM, Philips XL30 ESEM). Biofilm determination was performed as previously described [20]. The growth of biofilm was determined according methods in the available literature [21]. The physical characteristics of the MPC samples were measured in accordance with the sandstone pore structure method of image analysis. Archimedes law (i.e., any object placed in a fluid displaces its weight and an immersed object displaces its volume) is an accurate method for porosity measurement that we utilized [22].

3 Results and discussion

3.1 Effects of magnetic porous ceramsite (MPC) preparation

3.1.1 Effect of palygorskite

Figure 2 shows the effect of palygorskite on the compressive strength and porosity of MPC. Our study shows that: 1) when the content of palygorskite increases from 10 wt% to 50 wt%, the compressive strength increases from 2 N to 18 N and the porosity decreases from 84% to 76%; and 2) when the content of palygorskite increases from 50 wt% to 70 wt%, the compressive strength increases from 18 N to 61 N and the porosity decreases from 76% to 53%.

It should be noted that the effect of palygorskite content on the compressive strength is significant when the content is 50 wt% to 70 wt%. This result indicates that the increasing content of palygorskite improves the mechanical strength of MPC. The densification and melting of the MPC surface are possible reasons for the increase in the compressive strength of MPC with higher palygorskite ($Mg_5Si_8O_2O(OH)_2(H_2O)_4{\cdot}5H_2O$) contents (SiO_2 contents≥56.96%). This implies that the texture of MPC may play an important role in determining the compressive strength [23,24]. A study by Park and Heo indicated that as the content of palygorskite

increases, the bonding strength of metal ions increases which can enhance the compressive strength [25]. It should be noted that the effect of palygorskite contents on the porosity is significant when the content of palygorskite is 50 wt% to 70 wt%. This result indicates that the increase in palygorskite and sawdust (porosity) accounts for the decrease in porosity [26,27].

3.1.2 Effect of sawdust

Figure 3 shows the effect of sawdust on the compressive strength and porosity of MPC. Our study shows that there is a clear tendency for MPC to decrease in compressive strength as the amount of sawdust increases. When sawdust is raised from 0 wt% to 20 wt%, the compressive strength decreases from 59 to 45 N and the porosity increases from 3% to 67%. When sawdust is raised from 20 wt% to 50 wt%, the increased sawdust has a large effect on the compressive strength. Compressive strength decrease from 45 to 2 N, and the porosity increases from 67% to 90%. Reports indicate that sawdust could react with carbon to generate CO_2 [28]. The CO_2 product may diffuse or expand through the interior of the MPC particles, reducing the compressive strength [29]. This may explain the decreasing compressive strength with increasing sawdust when sawdust is a major component in MPC materials (Figure 2).

3.1.3 Effect of calcination temperature

Figure 4 shows the effects of calcination temperature on compressive strength and porosity of MPC. With an increase of calcination temperature from 400 $^{\circ}$C to 800 $^{\circ}$C, the compressive strength increases linearly from 20 N to 60 N. The compressive strength increased by 8 N with increases in calcination temperature from 700 $^{\circ}$C to 800 $^{\circ}$C. This indicates that MPC consolidation mechanisms like solid state and liquid phase sintering are not effective when the sintering temperature is below 500 $^{\circ}$C.

Figure 4 shows the porosity of MPC treated at different temperatures (400-800 $^{\circ}$C). The relationship between the sintering temperature and the porosity of MPC (25%-75%) is clear. After sintering at 400-800 $^{\circ}$C, a continuous increase in the porosity is observed. The MPC sintered at 700 $^{\circ}$C has the highest porosity (74%) and

compressive strength (52 N). At 800 °C there is a slight decrease in the porosity (74%-76%). In addition, the porosity of MPC after sintering is maximal. This implies that the adsorption and crystallization of water as well as the other adsorbed volatile compounds vanish from the as-received MPC (Fig. 7).

During sintering, the Si^{4+} is solidified in tectosilicate with a tetrahedron network of SiO_4^{4-} (Si-O-Si). The raw materials with a proper content of SiO_2 can enhance the formation of liquid phase at temperatures higher than 500 °C because the higher temperature encloses the solid particles and packs the pores in the solid particles [30-33]. Higher temperatures decrease the pores of MPC and improve the binding forces between the solid particles through the capillary action. The variation in SiO_2 contents can either also reduce the liquid phase in the MPC bodies, and it can make the MPC bodies denser with an increase in compressive strength that expands at temperatures above 500 °C [34]. During the MPC sintering process, palygorskite (Al_2O_3 contents 9.60%) is a skeleton material. The Al_2O_3 (contents 9.60%) can react with other components when temperatures are higher than 500 °C to form silicate mineral groups with relatively lower eutectic points, and the reaction effectively lowers the sintering point of the MPC and enhances the formation of the liquid phase [35]. The proper quantities of Al_2O_3 (9.60%) are beneficial to the liquid phase sintering at temperatures higher than 500 °C and improve the characteristics of MPC [36]. Our tests show that the calcination temperature has a great impact on the compressive strength from 500 °C to 700 °C.

3.1.4 Effect of calcination time

Figure 5 shows that the compressive strength increased by 10 N (from 48 N increased to 58 N) when the calcination is performed at 700 °C for 0.5-4.0 h. After 1 h, the MPC compressive strength reached 51 N. There are only slight increases as calcination time is extended from 1.5 h to 4 h.

Figure 5 shows different porosity time curves for MPC. When the calcination time increased (from 0.5 h to 3 h), the porosity of MPC increased from 50% to 69%. When calcined at 500 °C, the main forces affecting the porosity of MPC are water

molecules, sawdust, and decomposition of volatile substances. The effect of temperature on MPC diffusion is not obvious, but the effect of temperature on sawdust [$3C_6H_{10}O_5$] is known. MPC dehydration during calcination causes water evaporation. Thus, the space occupied by sawdust is emptied. This increases the porosity.

Excessive calcination time (4 h) causes the internal gas pressure to increase while the resistance is relatively low. The gases begin to escape more easily, and the internal microporous structure might be destroyed (Fig. 7) [37,38]. Therefore, the ideal calcination time should be 1 h to 3 h to achieve the ideal effects for compressive strength.

3.1.5 Analysis of orthogonal experiments

Goethite was the main component of the MPC tested. The palygorskite clay and sawdust were mixed with goethite to make the new type of MPC.

Five factors were considered in the MPC preparation: goethite dosage, ratio of palygorskite clay added, ratio of sawdust added, calcination temperature, and calcination time.

The ratio of palygorskite clay and sawdust added both depend on the goethite dosage. Orthogonal tests analyzed the influence of the five factors on the properties of MPC. The results show the optimized experimental conditions for the preparation of MPC (Tables 1-4).

An orthogonal $L_9 4^3$ test was used to optimize the particle preparation conditions. The evaluation index was analyzed statistically. The orthogonal test designs are listed in Table 2. Since we could not select the best preparation conditions based solely on the outcomes in Table 3, a further orthogonal analysis was warranted. Thus, the K_{mn} and R_n values were calculated. We found that the influence on the comprehensive index of MPC decreases in the following order: ratio of palygorskite clay added > calcination time > calcination temperature > ratio of sawdust added according to the R values ($R_1 > R_4 > R_3 > R_2$). The goethite dosage was found to be the most important determinant of preparation. The optimal preparation conditions of goethite were 100

g, palygorskite at 50 wt%, and sawdust added at 20 wt%. The calcination is optimized at 700 °C for 2 h (Table 4).

3.2 Magnetic porous ceramsite (MPC) characterization evaluation

The best preparation formula for MPC was a ratio of 10:2:5 (mass ratio) raw goethite, sawdust, and palygorskite clay. The optimal calcination temperature and time for MPC are 700 °C and 2 h. This formula met the Chinese national standards for MPC [22] (in Table 5). Contrast pictures of our synthesized MPC (left) and MPC are shown in Figure 9). The photographs illustrate MPC after magnetic separation, composite particles (Figure 9(a)), magnetic porous ceramsite (Figure 9(b)), and magnetic separation of the MPC (Figure 9(c)).

3.3 X-ray diffraction (XRD)and magnetic susceptibility

Figure 6 shows the XRD patterns of as-synthesized MPC and MPC (700 °C, 2 h). The main minerals in our synthesized MPC include quartz (SiO_2), palygorskite, and goethite (FeOOH) (see Figure 6a). In contrast, the main minerals in MPC (Fig. 6b) are quartz (SiO_2), hematite, palygorskite, and magnetite (Fe_3O_4). Comparing the results in Figure 6b shows that goethite has transformed into magnetic particles after sintering procession. The reflections at 2θ=9.8, 22.3, 27, and 32° are found and identified as MPC when compared with the standard JCPDS (89-6538). In addition, a new reflection at 2θ=26° was also found and identified as quartz. [39-42].

In this study, a mixture of goethite, sawdust, and palygorskite clay was thermally treated (under a N_2 atmosphere) to form MPC. The magnetic susceptibility of the MPC($X_{mass}=11690*10^{-8}m^3/kg$).

3.4 X-ray fluorescence (XRF) and Elemental analysis (EA)

The chemical compositions measured by EA indicate that the sawdust consisted of C 46.09%, H 6.85%, O 35.09%, N 0.6%, S 0.1%, as well as small amounts of Cl, P, K and Si. The chemical compositions measured by XRF indicate that the goethite consists of Fe 66.07%, Si 15.80%, Al 5.74%, Ca 1.57%, Mg 0.68%, Cr 0.03%, K

0.98%, P 0.07%, Na 0.24%, Pb 0.22%, Cu 0.46%, Mn 4.31%, as well as small amounts of As, S, Ba, Zr, Sr, Zn, Ni, and Ti. The chemical compositions measured by XRF indicate that the palygorskite consisted of SiO_2 55.10%, Al_2O_3 9.60%, Fe_2O_3 5.70%, Na_2O 0.05%, K_2O 0.96%, CaO 0.42%, MgO 10.70%, MnO 0.01%, and TiO_2 0.32%. No indication of heavy metals related to the analyzed material indicates that it is appropriate for filter media and microbial growth. Therefore, it is speculated that the presence of so many kinds of elements favors the growth of microorganism.

3.5 Composite particles morphological structures (SEM) analyses.

The SEM images of composite particles calcined at 700 °C for 4 h and composite particles calcined at 800 °C for 4 h are shown in Figure 7. The SEM observations show that the porous structures become more compact due to the increasing calcination time (4 h). The observations clearly show that the particulate nature of the crystals in the composite increases with calcination time. Bonding of sintered crystals is evident by the cohesive necks growing at the composite particle contact points (Fig. 7(a)). As seen in composite particles with calcination time of 700 °C for 4 h, there are abundant small pores with thin boundaries and large cracks with no boundary present on the surface. This is caused by the release of gases (Figure 7(a)). In Figure 7(b), the microstructure of the composite particle interior is seen after treatment at 700 °C for 4 h. The water absorption of the composite particles at 700 °C for 4 h remains relatively low despite the increasing number of pore space because the gas produced cannot create sufficient voids in the composite particle bodies. The gases begin to escape more easily and the internal microporous structure might be destroyed.

The surface of the composite particles treated at 800 °C for 4 h has few pores. The micrograph of these particles clearly shows that some micropores (6.0 µm pore size 10.0 µm) are irregularly distributed in the microstructure and macropores (Figure 7(c)). Melting phenomena are also observed on the crystalline surface of the composite particles treated at 800 °C for 4 h (Fig. 7(c)). The release of gases and melting of raw materials allow the large pores to form. The water absorption of the

composite particles treated at 800 °C for 4 h remains relatively low despite the larger pores because the impervious skin layer of the pellets restricts water ingress. The microstructure of these composite particles is also related to the lower viscosity of the liquid phase produced at 800 °C and the consequent improvement in densification during the natural cooling process. These results indicate that denser and lower porous ceramsite can be obtained via treatment at 800 °C for 4 h.

The increasing densification and neck growth between the calcined composite particles is seen in Figure 7(d) in the interior of the composite particles treated at 800 °C for 4 h. However, in Figure 7(d) the calcined composite particles samples show a clear internal micropore structure between the composite particles that might be destroyed, suggesting melted neck growth. The slight expansion of the composite particles that occurs when sintered at 800 °C is clearly associated with the formation of a significant number of approximately slit-shaped pores.

3.6 Magnetic porous ceramsite and commercial ceramsite under scanning electron microscopy (SEM)

Several typical SEM images of the ordered structure and biomass growth of MPC/commercial ceramsite are shown in Figure 8. In Figure 8(a), the appearance of a rough surface on MPC is a coral-like porosity structure providing shelter from the wastewater shear forces. As observed from Figure 8(a), plenty of macropores are formed on the surface of the internal surface which may serve as excellent locations for the colonization of microorganisms. In Figure 8(b), the microstructure of the internal surface and a cross-section of the MPC is seen. This indicates that the prepared MPC has a high number of pores with rectangular openings and pores interconnected to each other through a ladder-like structure as shown in Figure 8(a) and Figure 8(b). During sintering, macropores form inside the particles when sawdust is removed via combustion. MPC material with such porosity is suitable to serve as the biomedium in a BAF reactor.

The SEM images of the MPC after operation in the BAF reactor are provided in Figure 8(c) and Figure 8(d). The biofilm overlays on the surface of the MPC. Four kinds of bacteria can be observed: filamentous-shape, coral-shape, spherical, and

chain-shape (Fig. 8(c)). Obviously, the more diverse the bacterial community, the more organic pollutants are able to be biodegraded. After the growth of a bacterial population, a biofilm can be observed clearly on the surface of the internal porosity in Figure 8(d). At the start-up phase in the BAF reactor, the biofilms first develop when some bacteria irreversibly attach to the MPC. After more metabolites accumulate on the MPC surface, the MPC is completely covered by the biofilms, which are observed randomly on the surface. Our MPC has a high capacity for bacterial growth.

In Figure 8(e) the micrograph of commercial ceramsite (CC) clearly shows that pores with diameters ranging from 1.0 to 5.0 μm are irregularly distributed on the surface. There are some small pores and smooth surfaces. The microstructure in Figure 8(f) suggests that a small number of microorganisms are immobilized to the inside and outside surfaces of the pores in CC. The CC calcination temperature is 1200 °C. This will destroy the clay crystal structure of the main raw material, and the CC surface in high temperature calcination conditions is a crystalline glaze. The biofilm biomass and adsorption performance is poor which impacts the overall performance of this product [43].

3.7 Cast thin section of magnetic porous ceramsite (MPC)

In a BAF system, biofilter carriers play a significant role in meeting effluent quality requirements. The granular media is employed in the biofilter bed for solid interception and solid-liquid separation. The media is also the carrier of biofilm. The characteristics of the biofilter carriers have significant impacts on the treatment efficiency [44].

The roughness and porosity of the open MPC surface are beneficial for microorganisms fixed to the surface. The microbial biofilm attached to the MPC surface is a highly hydrophilic substance under conditions of constant flow of sewage. Environmental microorganisms can be transferred through the MPC into the interior pores (Fig. 10(a)), and the microbial biofilm can attach to the surface of the MPC. Wastewater flow can be divided into three layers: the aqueous adhesion layer, the aerobic layer, and the anoxic layer (Fig. 10(b)). The actions of the microorganisms in

the biofilm lead to this zonation and create the conditions for simultaneous nitrification and denitrification.

In order to obtain direct evidence of environmental microorganisms in open porosity of our MPC, rubber casting experiments were used to generate quantitative size and shape data from a thin section of pores. Figure 11(a) shows the intergranular pore textures observed in the thin section. The black sections denote calcined palygorskite biomass residues caused by carbonization while gray areas represent the intergranular pores of MPC. This demonstrates that MPC has a large volume of internal porosity, in which guest microbes can be accommodated. The size of those interconnected pores is approximately 40-65 μm (Fig. 11(A), 11(B), and 11(C)) and most bacteria are 0.5 μm or less in diameter. Thus, environmental microorganisms can achieve a sustained growth of population in the open porosity. When impregnated with blue-dyed epoxy (part B), the fully interconnected porosity with a diameter of 60 μm can be determined from the white section (part A). In fact, blue-dyed epoxy in the porosity system must overcome the capillary resistance of the throat size before they enter porosity space indicating the narrow composition of the pores.

3.8 Thermal Properties (DT-TG) Analyses.

Figure 12 presents the thermal analysis of the palygorskite clay/goethite/sawdust mixture. The DTA curve has 5 exothermic valleys and an exothermic peak. According to the crystal structure of the palygorskite clay and crystal chemical formula, the water in palygorskite clay has four states including water adsorbed to the outer surface, water adsorbed in tunnels, water contained in the crystal structure, and structural water molecules coordinated to Mg(II) cations at the edge of the octahedral sheets [45]. The first endothermic valley is at 65 °C. This belongs to the water adsorbed to the outer surface and has a dehydrating effect. The second endothermic valley is at 98 °C, the thermal effect of adsorbed water in channels emerge and the weight of the adsorbed water on the outer surface and in pores is 5.87%. The third endothermic valley is at 230 °C and represents the crystal water absorbing effect produced by extrusion. It has a small and narrow endothermic

valley with 3.12% water loss. The fourth endothermic valley at 481 °C is wider and corresponds to the crystal degradation under thermal effects. It is a 3.7% loss. The fifth endothermic valley is at 595 °C, corresponding to the degradation of crystal structure. The amount of dehydration is 5.3%.

3.9 Determination of biomass in media.

To investigate the performance of MPC and commercial ceramsite in the BAF reactor, the biomass of grown biofilm was determined. The biofilm biomass was 54.1 mg TN/g for MPC and 2.2 mg TN/g for commercial ceramsite [46]. Also, the structural and morphological characteristics of the porous media, seen in Figure 8 and Figure 11, proved that the MPC surface and internal pores are advantageous to microbial growth under the conditions tested.

4. Conclusions

(1) The MPC can be prepared from a mixture of goethite, sawdust, and palygorskite by sintering at 700 °C for 120 min. The proper mass ratio of goethite, sawdust, and palygorskite is 10:2:5. The results indicate that MPC has a larger specific surface area (81 m^2/g). It has a porosity of 78% and a compressive strength range of 53-67 N, compared to commercial ceramsite (CC), which is superior to the regulatory levels in the Chinese National Standards.

(2) In the preparation of MPC, the goethite can be transformed into magnetite particles. Thus, this kind of ceramsite is a magnetic material. Furthermore, SEM and PM results suggest that the uniform and interconnected pores in MPC are suitable for microbial growth. Experimental growth of biofilm in this material is superior to that on CC. It is speculated that these observations will favor the utilization of MPC in the biotreatment of BAF.

Acknowledgements

We gratefully acknowledge the support by the National Natural Science Foundation of China (41072036, 41130206, 41372045), the Specialized Research Fund for the Doctoral Program of Higher Education of China (20110111110003), and the Anhui Provincial

Natural Science Foundation (11040606Q30)

References

[1] Yu YZ, Feng Y, Qiu LP, Effect of grain-slag media for the treatment of wastewater in a biological aerated filter, Bioresou Technol. 99 (2008) 4120–4123.

[2] Qiu LP, Ma J, Zhang LX, Characteristics and utilization of biologically aerated filter backwashed sludge, Desalination. 208 (2007) 73–80.

[3] Sang JQ, Zhang XH, Li LZ, et al. Improvement of organics removal by bioceramsite filtration of raw water with addition of phosphorus,Water Res. 37 (2003) 4711-4718.

[4]Shen YJ, Wu GX, Fan YB, et al. Performances of biological aerated filter employing hollow fiber membrane segments of surface-improved ploy (sulfone) as biofilm carriers, J Environ Sci. 19 (2007) 811-877.

[5] Salehi E, Abedi J, Harding T, Bio-oil from sawdust: pyrolysis of sawdust in a fixed-bed system, Energy Fuels. 23 (2009)3767–3772.

[6] Ji GD, Zhou Y, Tong JJ. Nitrogen and phosphorus adsorption behavior of ceramsite material made from coal ash and metallic iron, Environ Eng Sci. 27(2010)871-878.

[7] Lu XX, Song JM, Li XG, et al. Geochemical characteristics of nitrogen in the southern yellow sea surface sediments, J Mar Syst. 56 (2005)17-27.

[8] Liu HB, Chen TH, Chang J, et al. The effect of hydroxyl groups and surface area of hematite derived from annealing goethite for phosphate removal, J Colloid Interf Sci. 398 (2013)88-94.

[9]Fangqun Gan, Jianmin Zhou, Huoyan Wang, et al. Removal of phosphate from aqueous solution by thermally treated natural palygorskite, Water Res. 43 (2009)2907-2915

[10]Hirsiger W, Muller-Vonmoos M., Wiedemann H.G., Thermal analysis of palygorskite, Thermochim. 13(1975) 223-230.

[11]Jha V.K., Kameshima Y., Nakajima A., Utilization of steel-making slag for the uptake of ammonium and phosphate ions from aqueous solution, J. Hazard. Mater. 156 (2008)156-162.

[12]Yavuza H, Celebi SS, Effects of magnetic field on activity of activated sludge in wastewater treatment, Enzyme Microb Technol. 26(2000) 22-27.

[13] Goodman EM, Greenebaum B, Marron MT. Magnetic fields after translation in Escherichia coli, Bioelectromagnetics. 15 (1994) 77-83.

[14] Tabrah FL, Mower HF, Batkin S, Greenwood PB. Enhanced mutagenic effect of a 60 Hz time-varying magnetic field on numbers of a zide-induced TA100 revertant colonies, Bioelectromagnetics. 15(1994) 85-93.

[15] Ozaki H, Liu Z, Terashima Y. Utilization of microorganisms immobilized with magnetic particles for sewage and wastewater treatment, Wat Sci Tech. 23(1991) 1125-1136.

[16]Jung J, Sanji B, Godbole S, Sofer S. Biodegradation of phenol. A comparative study with and without applying magnetic fields, J Chem Tech Biotechnol. 556(1993) 73-76.

[17]Daou TJ, Begin-Colin S, Grene MJ, Phosphate adsorption properties of magnetite-based nanoparticles, Chem Mater. 19(2007) 4494-4505.

[18] Zou JL, Xu GR, Pan K, Nitrogen removal and biofilm structure affected by COD/NH_4^+–N in a biofilter with porous sludge ceramsite, Sep Purif Technol. 94(2012) 9-15.

[19] Zou XH, Chen TH, Liu HB, et al. Structural and chromatic evolution of goethite by thermal treatment, J Chinese Ceramic Society. 41(2013) 669-673(in Chinese).

[20] Zhu YR, Zhang RY, Wu FC, Distribution of bioavailable nitrogen and phosphorus forms and their relationship in the sediments of Dianchi Lake, Res Environ Sci. 8(2010) 994-998 (in Chinese).

[21] Sandstone pore structure method of image analysis(Industry standard CJ/T) (in Chinese).

[22] Chinese Mohurd, Artifical ceramsite filter material for water treatment, China standard publishing house, Beijing, China, 2008.

[23] Xu GR, Zou JL, Li GB, Ceramsite made with water and wastewater sludge and its characteristics affected by SiO_2 and Al_2O_3, Environ. Sci. Technol. 42(2008) 7417-7423.

[24] Park YJ, Heo J, Vitrification of fly ash from municipal solid waste incinerator, J Hazard Mater. 91(2001) 83-93.

[25] Toya T, Kameshima.Y, Yasumori. A, Preparation and properties of glass-ceramics from wastes (Kira) of silica sand and kaolin clay refining, J Eur Ceram Soc. 24(2004) 2367-2372.

[26] Yilmaz O, Unlu K, Cokca E, Solidification/stabilization of hazardous wastes containing metals and organic contaminants, J Environ. Eng. 129(2003) 366-376.

[27] Li CT, Lee WJ, Huang KL, Vitrification of chromium electroplating sludge, Environ. Sci. Technol. 41(2007) 2950-2956.

[28] Gutsey GL, Mochena MD, Structure and properties of Fe^4 with different coverage by C and CO, J. Phys. Chem. 108(2004) 11409-11418.

[29] Chen Y, Lin B, Research on enzyme immobilization by modified ceramsite particle, Chem Indus Eng Pro. 10(2008) 1462-1478. (in Chinese).

[30] Huang CP, Pan JRS, Liu YR, Mixing water treatment residual with excavation waste soil in brick and artificial aggregate making, J. Environ. Eng. 131(2005) 272-277.

[31] Tay JH, Hong SY, Show KY, Reuse of industrial sludge as palletized aggregate for concrete, J. Environ. Eng. 126 (2000) 279-287.

[32] Shih K, White T, Oleckie J, Spinel formation for stabilizing simulated nickel laden sludge with aluminum rich ceramic precursors, Environ. Sci. Technol. 40(2006) 5077-5083.

[33] Xu GR, Zou JL, Li GB, Effect of sintering temperature on the characteristics of sludge ceramsite, J Hazard Mater. 150(2008) 394-400.

[34] Xu GR, Zou JL, Li GB, Stabilization of heavy metals in ceramsite made with sewage sludge, J Hazard Mater. 152(2008) 56-61.

[35] Xu GR, Zou JL, Dai Y, Utilization of dried sludge for making ceramsite, Water Sci Technol. 54(2006) 69-79.

[36] Xu GR, Zhang WT, Li GB, Adsorbent obtained from CEPT sludge in wastewater chemically enhanced treatment, Water Res. 39(2005) 5175-5185.

[37]Fuliana A, Conesa JA, Font R, Formation and destruction of chlorinated

pollutants during sewage sludge incineration, Environ Sci Technol. 38(2004) 2953-2958.

[38] Mukherjee PS, Lokanatha S, Bhattacherjee S, High temperature structural studies in palygorskite, J. Mater. Sci. 26(1991) 6073-6077.

[39] Frost R., Ding Z., Ruan H., Thermal analysis of goethite, J Thermal Anal Calorim. 71(2003) 783-791.

[40] Gualtieri A. F., Venturelli P, In situ study of the goethite-hematite phase transformation by real time synchrotron powder diffraction, Am. Mineral. 84(1999) 895-904.

[41] Prasad P.S.R, Shiva Prasad K., Krishna Chaitanya V., In situ FTIR study on the dehydration of natural goethite, J. Asian Earth Sci. 27(2006) 503-511.

[42] Ozdemir O, Dunlop D.J., Earth Planet Intermediate magnetite formation during dehydration of goethite, Sci. Lett. 177(2000) 59-67.

[43] He S, Xue G, Kong H, The performance of BAF using natural zeolite as filtermedia under conditions of low temperature and ammonium shock load, J Hazard Mater. 143 (2007) 291-295.

[44] Han S, Yue Q, Yue M, et al. The characteristics and application of sludge fly ash ceramic particles (SFCP) as novel filter media, J Hazard Mater. 171(2009) 809-814.

[45] Chen Tianhu, Wang Jian, Qing Chengsong, et al. Effect of heat treatment on structure ,morphology and surface properties of palygorskite, J Chinese Ceramic Society (in Chinese).34(2006) 1407-1410.

[46] Ha JH, Ong SK, Nitrification and denitrification in partially aerated biological aerated filter (BAF) with dual size sand media, Water Sci Technol. 55(2007) 9-17.

List of Figures

Fig. 1 Schematic diagram of the BAF system

(A) MPC BAF; (B) Effluent pipe; (C) Air blower; (D) Wastewater pump; (E) Switching mode power supply; (F) Electromagnetic iron-separator device; (G) Wastewater tank

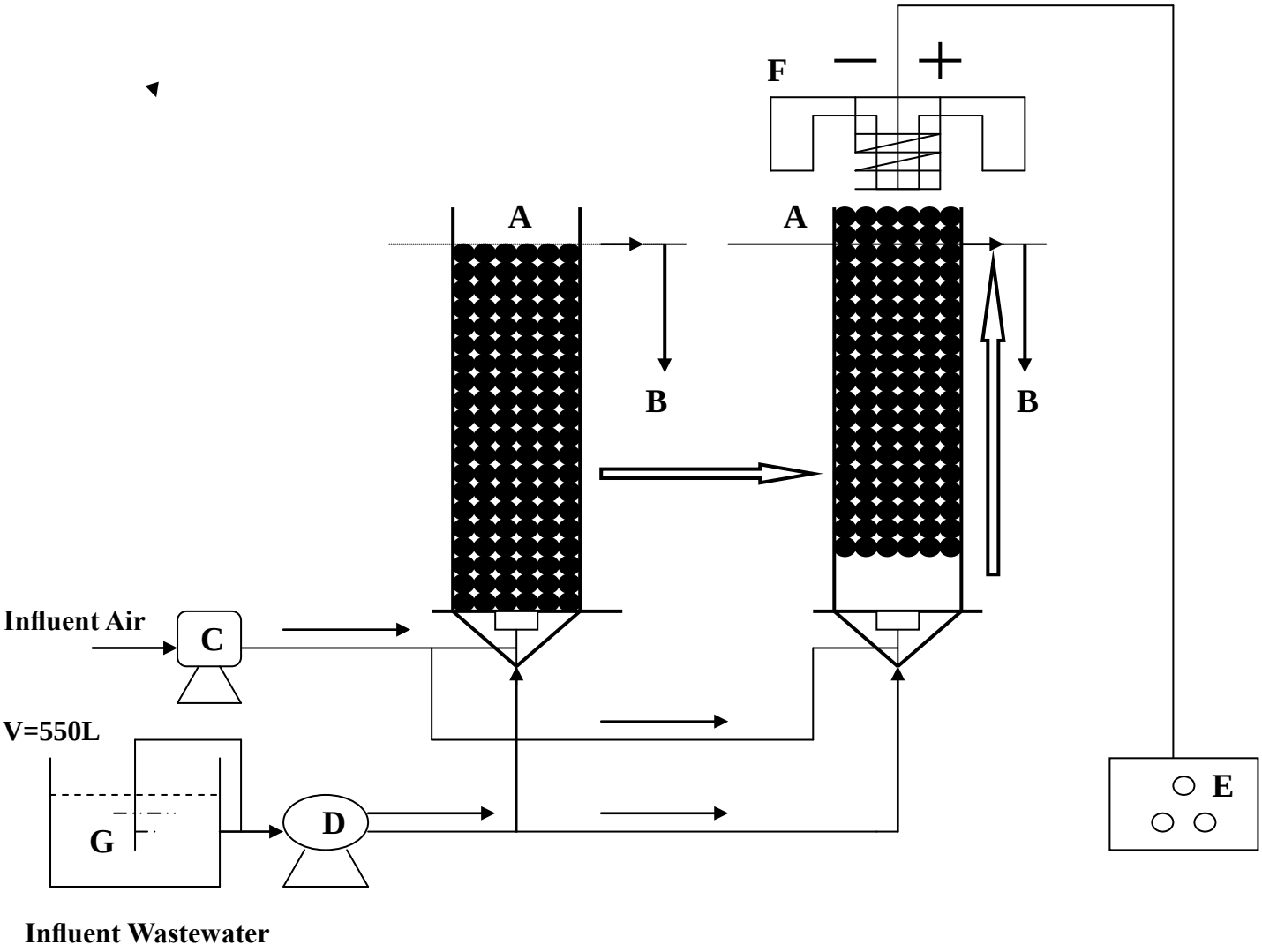

Fig. 2 The effect of palygorskite clay addition on compressive strength and porosity of MPC.

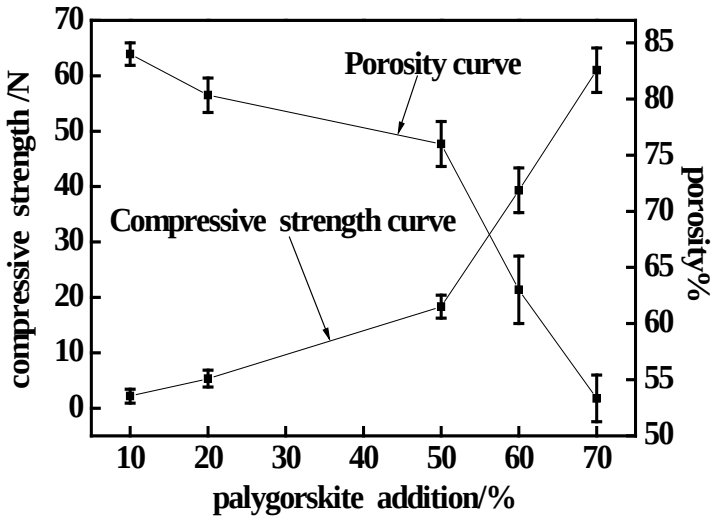

Fig. 3 The effect of sawdust addition on compressive strength and porosity of MPC.

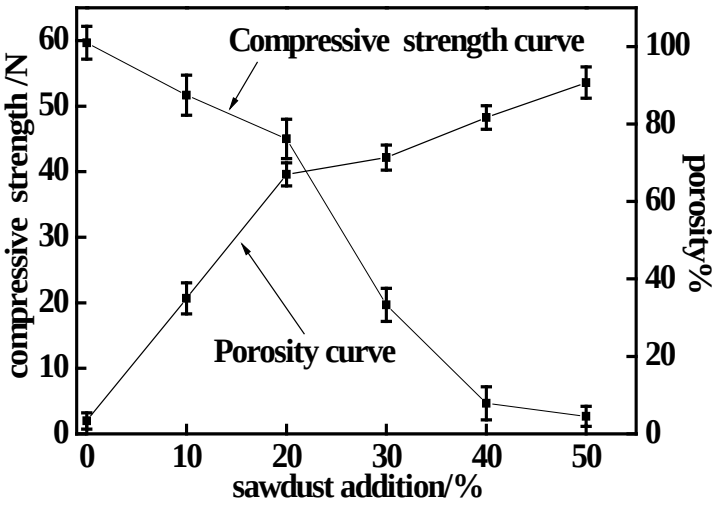

Fig. 4 MPC compressive strength and porosity as a function of calcination temperature.

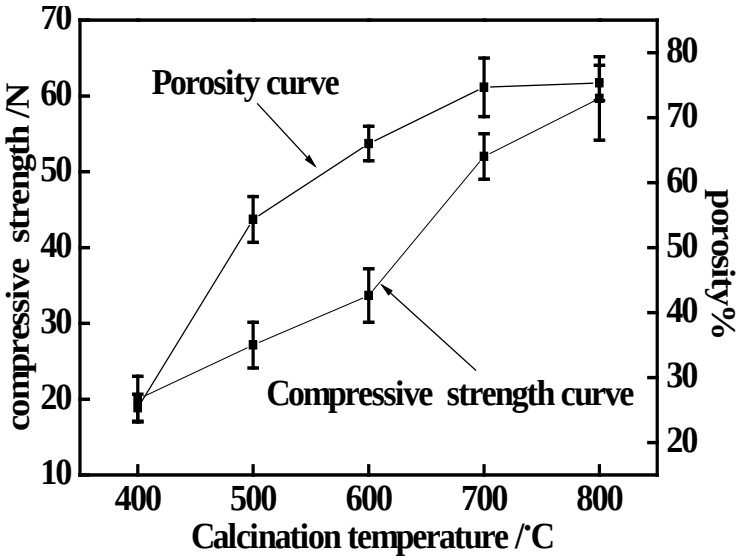

Fig. 5 MPC compressive strength and porosity as a function of calcination time.

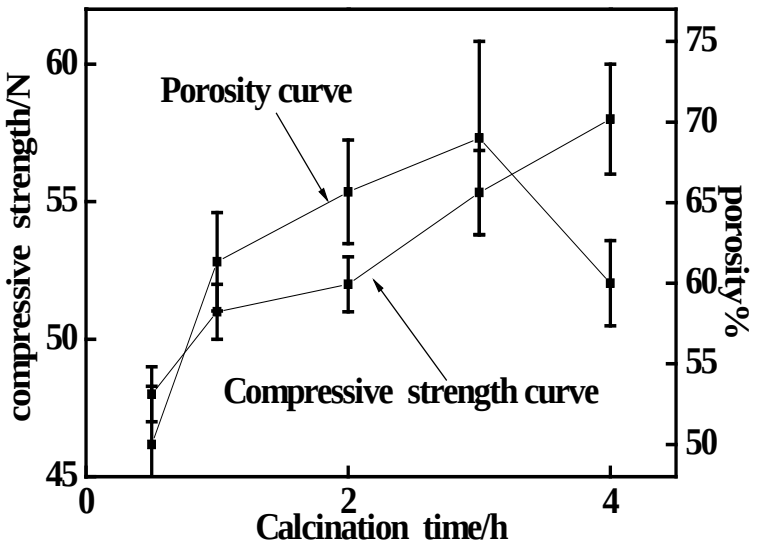

Fig. 6 X-ray diffraction patterns of composite particles and MPC

(a) Composite particles; (b) MPC

(P: palygorskite; Q: quartz; M: magnetic; H: hematite)

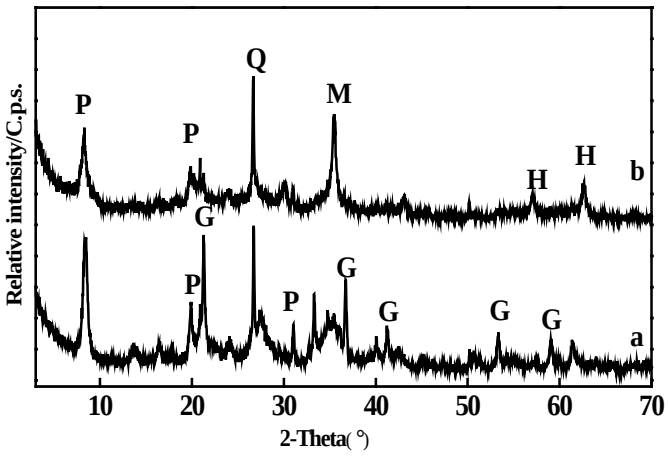

Fig. 7 SEM images of composite particles calcined at 700 °C for 4 h and composite particles calcined at 800 °C for 4 h.

(a) raw external surface of composite particles calcined at 700 °C for 4 h

(b) raw internal surface of composite particles calcined at 700 °C for 4 h

(c) raw external surface of composite particles calcined at 800 °C for 4 h

(d) raw internal surface of composite particles calcined at 800 °C for 4 h

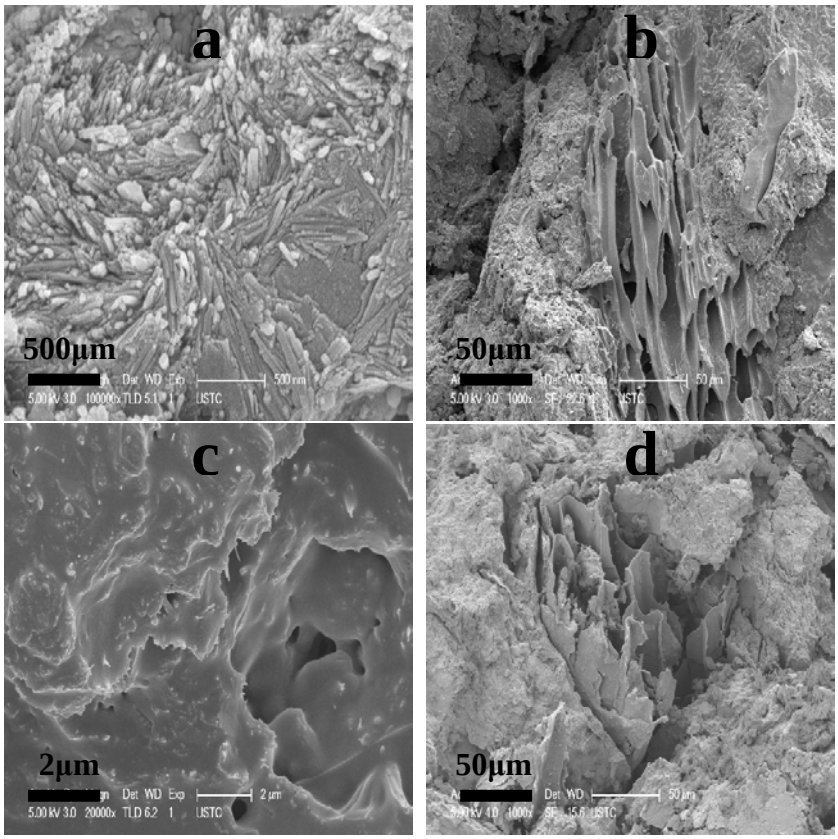

Fig. 8 SEM images of MPC/commercial ceramsite

(a) raw external surface of MPC

(b) raw internal surface of MPC

(c) microbial load on external surface of MPC

(d) microbial load on internal surface of MPC

(e) raw external surface of CC

(f) microbial load on external surface of CC

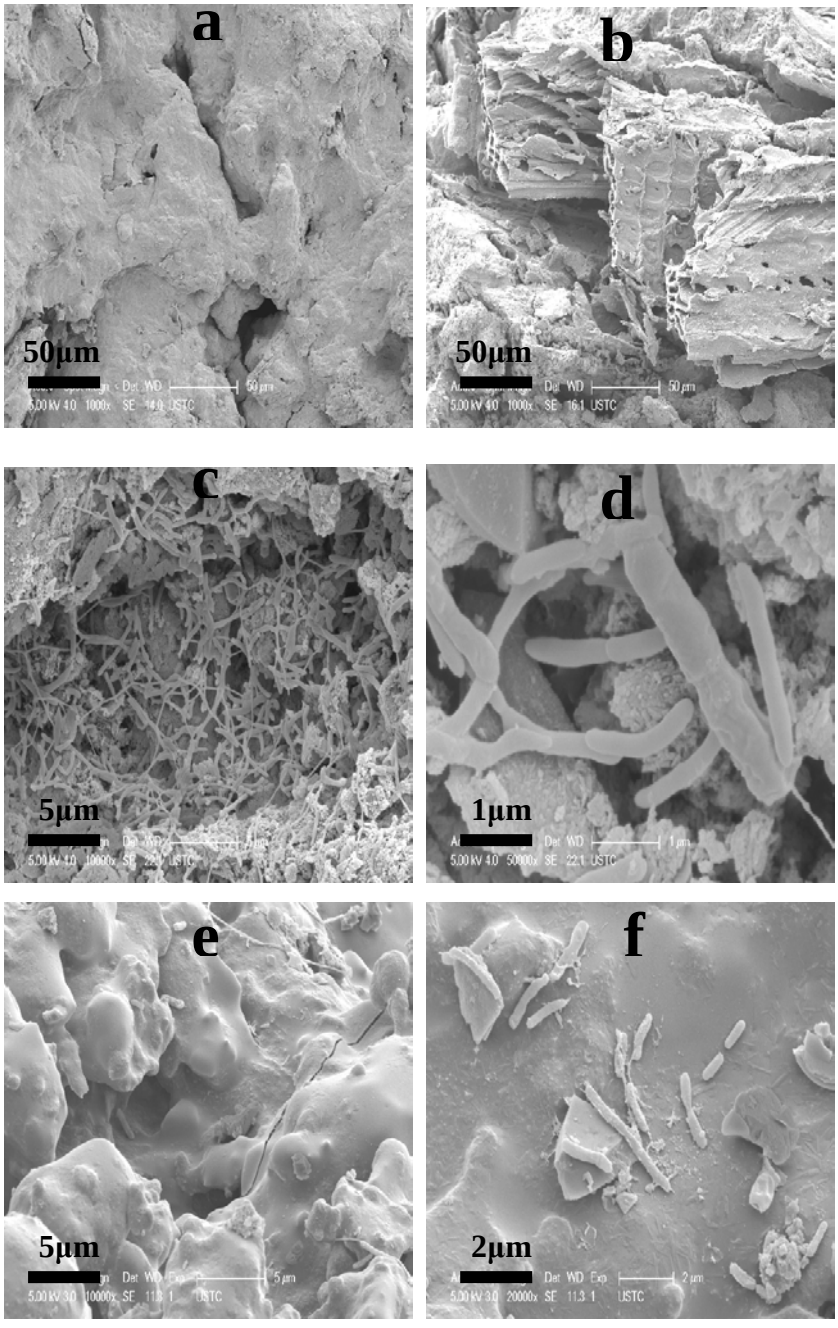

Fig. 9 Contrast pictures of composite particles (left) and MPC (right) photographs after magnetic separation of the MPC

(a) composite particles; (b) MPC; (c) magnetic separation of the MPC;

Fig. 10 Internal images of MPC.

(a) Internal porosity of MPC; (b) Layers of MPC when oxygen is introduced into the system;

(1. aqueous adhesion layer; 2. aerobic layer; 3. anoxic layer)

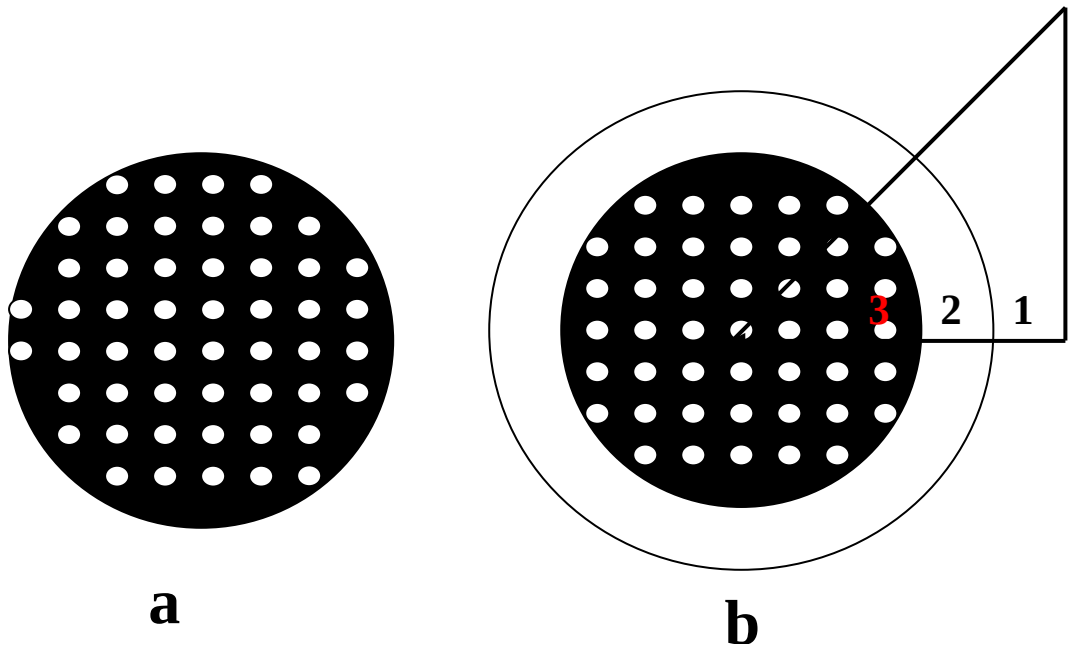

Fig. 11 Porosity of MPC.

(a) After calcination (gray – MPC) (b) Filled (dark blue – open pores)

(c) A higher resolution image illustrating the internal surface of MPC (dark blue – open pores)

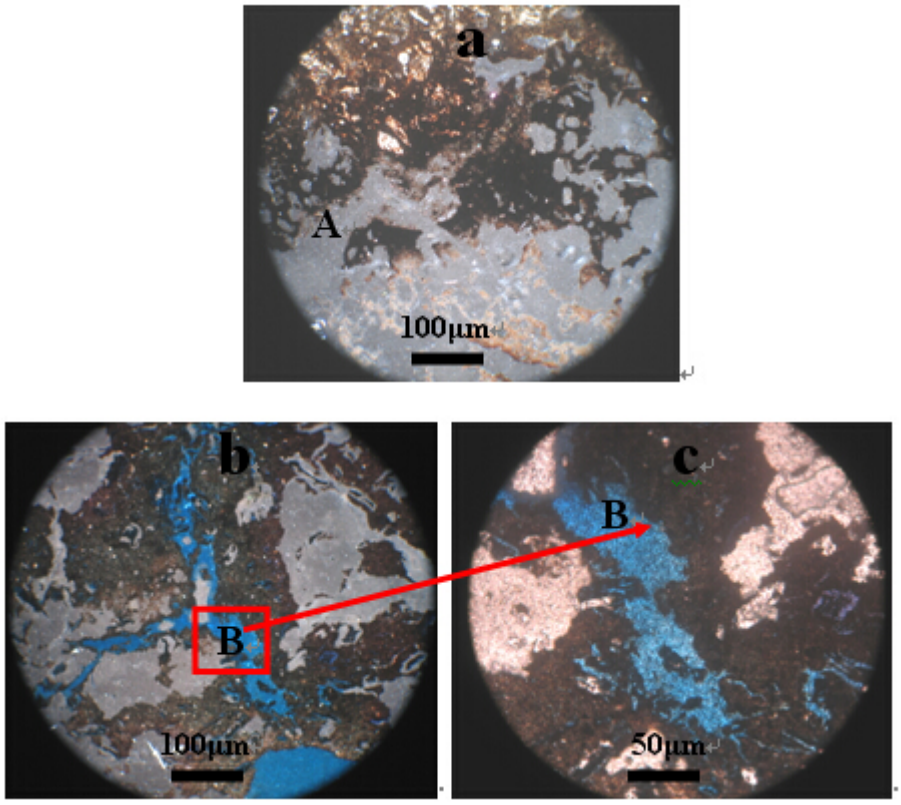

Fig. 12 Differential thermal analysis and thermogravimetric analysis patterns of MPC

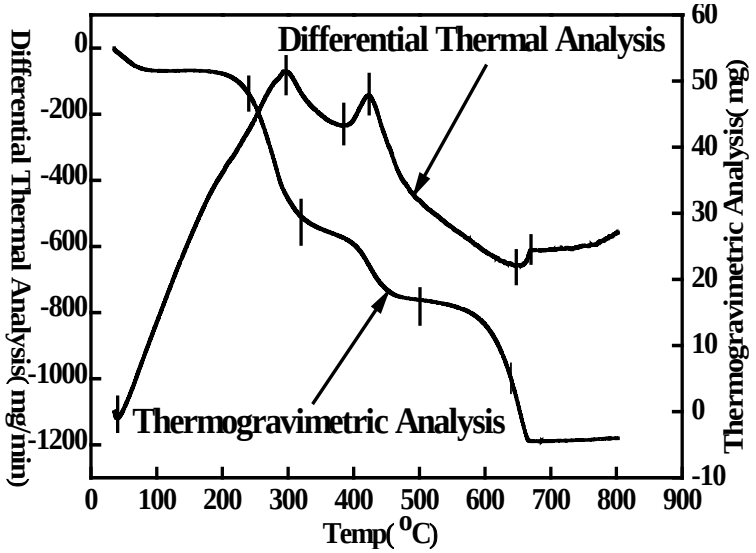

List of Tables

Table 1 Factors and levels of the orthogonal experimental design.

Note: the proportion of palygorskite and sawdust is accounted for in goethite content percent.

(A), The level. (B), The amount of palygorskite (wt% GT). (C), Sawdust dosage (wt% GT). (D), Calcination temperature (°C). (E), Calcination time (h)

A_n	B_n	C_n	D_n	E_n
i	B_1	C_1	D_1	E_1
ii	B_2	C_2	D_2	E_2
iii	B_3	C_3	D_3	E_3

Table 2 Factors and levels values for the orthogonal experiments.

A_n	B_n	C_n	D_n	E_n
i	50 wt% GT	20 wt% GT	500°C	1h
ii	60 wt% GT	30 wt% GT	600°C	2h
iii	70 wt% GT	40 wt% GT	700°C	3h

Table 3 Design of orthogonal experiments.

Note: Ki indicates the level of compression strength, R is the difference between the largest average effect and minimum average effect for every factor, A_n is the Orthogonal experiment number, B_n is Palygorskite (wt% GT), C_n is Sawdust (wt% GT), D_n is Calcination temperature (°C), E_n is Calcination time (h), and F_n is Compression strength (N).

	A_n	B_n	C_n	D_n	E_n	F_n
	i	B_1	C_1	D_1	E_1	$B_1C_1D_1E_1$
	ii	B_1	C_2	D_2	E_2	$B_1C_2D_2E_2$
	iii	B_1	C_3	D_3	E_3	$B_1C_3D_3E_3$
	iv	B_2	C_1	D_2	E_3	$B_2C_1D_2E_3$
	v	B_2	C_2	D_3	E_1	$B_2C_2D_3E_1$
	vi	B_2	C_3	D_1	E_2	$B_2C_3D_1E_2$
	vii	B_3	C_1	D_3	E_2	$B_3C_1D_3E_2$
	viii	B_3	C_2	D_1	E_3	$B_3C_2D_1E_3$
	ix	B_3	C_3	D_2	E_1	$B_3C_3D_2E_1$
	K_{1n}	K_{11}	K_{12}	K_{13}	K_{14}	
F	K_{2n}	K_{21}	K_{22}	K_{23}	K_{24}	
	K_{3n}	K_{31}	K_{32}	K_{33}	K_{34}	
	R_n	R_1	R_2	R_3	R_4	

Table 4 Results of orthogonal experiments.

A		B_n	C_n	D_n	E_n	F_n
1		50 wt% GT	20 wt% GT	500 ℃	1 h	49.40
2		50 wt% GT	30 wt% GT	600 ℃	2 h	51.13
3		50 wt% GT	40 wt% GT	700 ℃	3 h	52.14
4		60 wt% GT	20 wt% GT	600 ℃	3 h	45.12
5		60 wt% GT	30 wt% GT	700 ℃	1 h	40.15
6		60 wt% GT	40 wt% GT	500 ℃	2 h	38.27
7		70 wt% GT	20 wt% GT	700 ℃	2 h	58.65
8		70 wt% GT	30 wt% GT	500 ℃	3 h	40.23
9		70 wt% GT	40 wt% GT	600 ℃	1 h	34.78
	K_1	50.89	51.06	42.63	41.32	-
F	K_2	41.18	43.84	43.68	49.35	-
	K_3	44.55	43.55	50.31	45.83	-
	R_n	9.71	7.51	7.68	8.03	-

Table 5 The regulatory levels of ceramics in MPC and CC as well as the corresponding Chinese National Standards.

Item	Chinese National Standard	MPC experimental levels	CC experimental levels
Grain diameter, d/mm	0.5-9.0	3-5	4-6
Silt carrying capacity, C_s/%	≤1	0.17	≤1
Solubility in hydrochloric acid, C_{ha}/%	≤2	1.15	≤1.5
Void fraction, υ/%	≥40	76.31	＞42
Specific surface area, S_w/cm^2/g	$\geq 0.5\times10^4$	8.1×10^5	$\geq 2\times10^4$
Piled density, ρ_p/g/cm^3	--------	0.617	≤1.0
Apparent density, ρ_{ap}/g/cm^3	---------	1.611	1.4-1.8
Compression strength, /N	---------	53-67	≥87
Porosity, P/%	---------	78	--